

# Userfriendly two-photon microendoscope for *in vivo* imaging

---

*A bachelor research  
report*

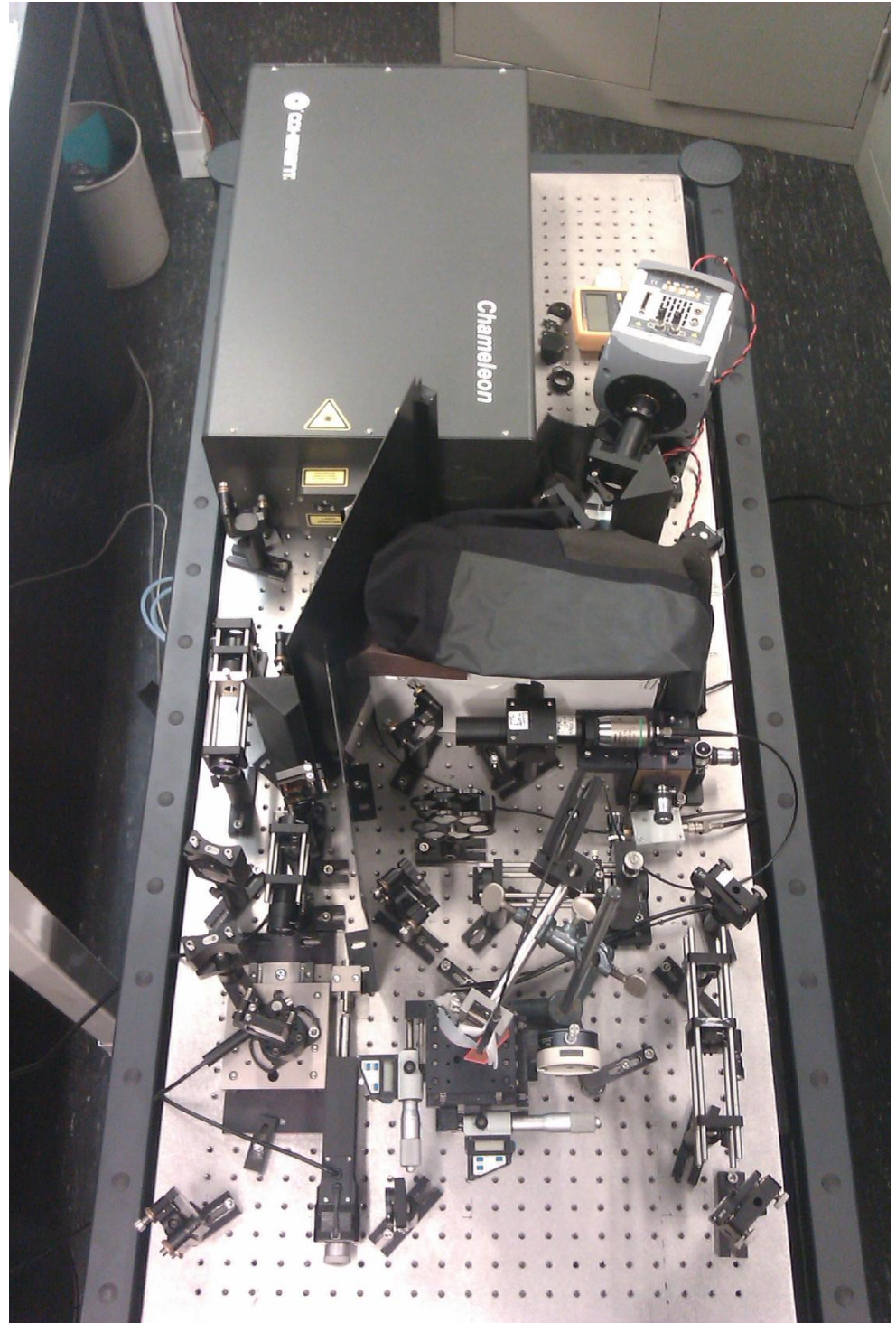
July 5<sup>th</sup> 2012

Celine Alkemade

Under supervision of  
MSc. C.J. van Voskuilen  
Prof. Dr. H.C. Gerritsen

Utrecht University

At the  
Department of Physics  
Molecular Biophysics



This report describes my research on a two-photon fluorescence microendoscope (3 mm outer diameter) for in vivo imaging of a 175x175  $\mu\text{m}$  field of view. First I discuss two-photon fluorescence and second harmonic generation and how they can be used for imaging. I also discuss the biological relevant molecules we will image and how that is possible with spectral imaging. Then I discuss the goal of my bachelor research and I discuss the components of the set-up in detail. Thereon I present the results of both the regular benchtop set-up as the mobile set-up and I conclude with ideas for further research and a conclusion.

## Contents

1. Introduction	page 3
2. Theoretical Background	page 3
2.1. Two-photon fluorescence	page 3
2.2. Second Harmonic Generation	page 4
2.3. NADH, cancer cells and collagen	page 5
2.4. Spectral imaging	page 5
3. Experiment	page 7
4. Mobile Set-up	page 8
4.1. Laser	page 9
4.2. Attenuator	page 9
4.3. Beam Expander	page 9
4.4. GVDC	page 9
4.5. Beam Compressor and Spatial-mode Fiber	page 11
4.6. Dichroic Mirror	page 11
4.7. Fiber	page 12
4.8. Scanner	page 13
4.9. PMT detector	page 13
4.10. Prism and CCD camera	page 14
5. Results	page 15
5.1. Regular benchtop set-up	page 15
5.2. Mobile set-up	page 16
6. Further research	page 18
7. Conclusion	page 18
8. Acknowledgements	page 18
9. Appendix	page 19
9.1. Periodic check	page 19
9.2. Constant height beam	page 19
9.3. Central alignment beam	page 19
9.4. Optimizing pinholes and fiber coupling	page 20
10. References	page 21

## 1. Introduction

Nonlinear multiphoton fluorescence microscopy is an important imaging technique to visualize cell structures. With this microscopy it is possible to image different cellular layers of tissue in a noninvasive way and therefore to study *in vivo* molecular mechanisms<sup>1,2,3</sup>. This optical biopsy can also be used for medical diagnostics. It will be less invasive than incisional biopsy and it will give immediately results about the tissue. This means results are minimally one week earlier available.

We have developed a userfriendly handheld two-photon fluorescence microendoscope for *in vivo* imaging, which will be used in a clinic (Erasmus Medical Centre) for further research of the development of cancer cells. The compact handheld probe of the two-photon endoscope can be easily brought into contact with the target tissue and the optical and electronic hardware is placed on a mobile table of 0.6 m by 1.5 m.

## 2. Theoretical Background

### 2.1 Two-photon fluorescence

Fluorescence is the emission of light which occurs in excited (singlet) states, when the electron in the excited orbital is paired (by opposite spin) with a second electron in the ground state orbital. While emitting a photon, the excited electron returns to the ground state quickly, because this state is spin allowed<sup>4</sup>. To get the electron in this excited state it needs to have sufficient energy, which it will have when absorbing a photon. Fig. 1(a) displays a Jablonski energy diagram of the excitation of an electron from its ground state to the first electronic excited state and the fluorescence emission of a photon, taken from So e.a. (2000)<sup>5</sup>

In this research the electron will be excited by two photons. Fig. 1(b) shows a Jablonski energy diagram of such an excitation and fluorescence. This excitation is nonlinear with the power and will only take place in the laser focal point of the tissue, so only at a certain depth. Therefore one can get very clear images of the different layers of the tissue. Another advantage of two-photon fluorescence is its reduced effect of photodamage, so it allows imaging of living specimens. Also, with two-photon fluorescence one can use near infrared light, which is able to penetrate much deeper into tissue than smaller wavelengths (up to several hundreds of  $\mu\text{m}$ )<sup>5</sup>.

If saturation is neglected and the paraxial approximation is assumed (so  $\sin \theta \approx \theta$ ), the average number of absorbed photons per fluorophore per pulse  $n_a$  depends, as shown by Denk e.a. (1990)<sup>6</sup>, as

$$n_a \approx \frac{p_0^2 \sigma}{\tau_p f_p^2} \left( \frac{NA^2}{2\hbar c \lambda} \right)^2$$

where  $c$  is the speed of light,  $\hbar$  the reduced Planck constant,  $p_0$  the laser power,  $\sigma$  the two-photon cross section,  $\tau_p$  the pulse width,  $f_p$  the pulse frequency,  $NA$  the lens numerical aperture and  $\lambda$  the pulse wavelength.

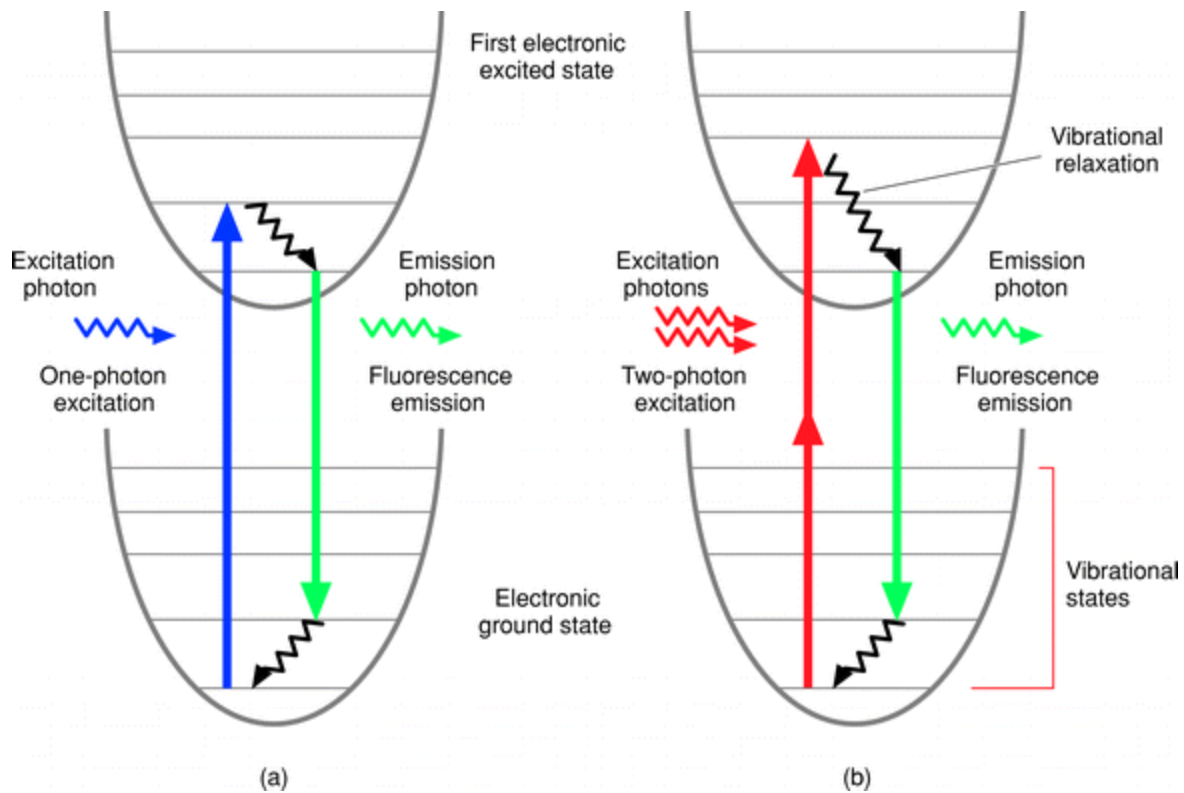


Figure 1: Jablonski energy diagram of one-photon (a) and two-photon (b) excitation of the electron from its ground state to the first electronic excited state. (So *et al*, 2000)<sup>5</sup>.

Two-photon fluorescence is used in imaging and microscopy by analyzing the emission signal. Because of the existence of intrinsic fluorophores, one can image the location of the molecule without staining and one can identify the molecule by analyzing its emission signal.

## 2.2 Second Harmonic Generation

Second harmonic generation (SHG) is an effect which arises when photons interact with a nonlinear material. The material will combine the photons in such a way that they will have twice the energy of the initial photons, as can be seen in Fig. 2. This means that they will have half the wavelength of the initial photons and can therefore be detected. Depending on the material, the largest part of this signal will go through the nonlinear material and only a small part will scatter backwards. However, the intensity of this signal is still high enough to detect.

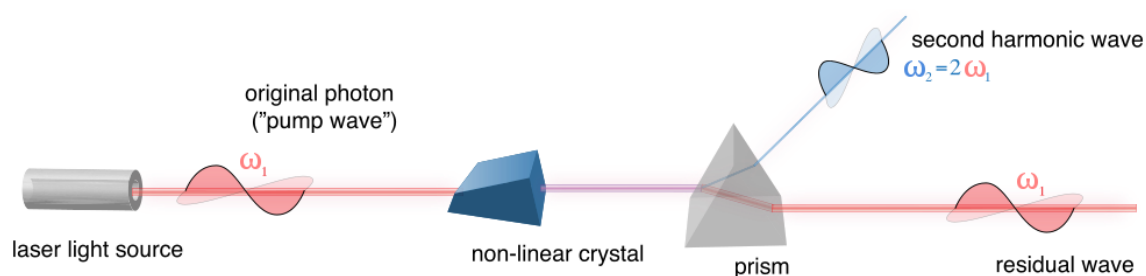


Figure 2: Second harmonic generation (taken from Wikipedia)<sup>7</sup>.

There is a big difference between the SHG signal and the two-photon fluorescence signal: the bandwidth of the SHG signal is in the order of the laser pulse ( $\sim 5$  nm), while the bandwidth of the fluorescence signal is much wider, because of the different vibrational levels of the electron, shown in Fig. 1, and the emission photon has therefore a lower energy as the excitation photon(s). Because of this difference in signal, the SHG signal can also be used for imaging. With the existence of non-linear proteins like collagen, one can image the location of those molecules without staining and one can identify the molecule by analyzing its reflected signal.

### 2.3 NADH, cancer cells and collagen

Within the cells of living organism, a lot of complicated chemical reactions take place. Together these are called the cell's metabolism and they allow the cell, and thus the organism, to grow. One of these processes involves the coenzyme NADH (reduced nicotinamide adenine dinucleotide), which transfers and donates electrons and thus energy. This coenzyme is formed from  $\text{NAD}^+$  during a metabolic cycle in which energy is extracted from complex molecules (like the glycolysis cycle). The NADH is oxidized back into  $\text{NAD}^+$  by reducing the present  $\text{O}_2$  and thereby producing water ( $\text{H}_2\text{O}$ ) and energy. This, however, is in a cell with high metabolism a slower process than the forming of NADH, because of the need of  $\text{O}_2$ <sup>8</sup>. This means that when there is a lot of activity in the cell, the amount of NADH will be higher due to the energy needed in the cell. Because NADH is an intrinsic fluorophore, it is possible to measure the amount of NADH in a cell by two-photon fluorescence and thereby gain information on a cell's metabolism.

An example for high-metabolism cells are cancer cells and its observation is called the Warburg effect<sup>9</sup>. These cells undergo unrestrained mitosis and grow very fast. During the mitosis the DNA is duplicated, which costs energy, and specifically the growing costs lots of energy. One could expect a high concentration of NADH in these cells. By examining the amount of NADH we might be able to detect cancer cells and do further research on these cells.

Another important protein for this experiment is collagen. Collagen is mostly found in fibrous tissue, such as skin, and its morphology is changed by cancer cells<sup>10</sup>. Since collagen is a nonlinear material, we will be able to image these structural changes with the SHG signal, and consequently image the cancer cells.

### 2.4 Spectral imaging

Spectral imaging is an imaging method which is used to collect information about the spectrum of each pixel. With this information, one can make a distinction between different fluorophores and consequently different particles. An example of such a spectrum is displayed in Fig. 3, which shows the emission (solid curve) and excitation (dotted curve) spectra of Alexa Fluor. Alexa Fluor is a commonly used fluorophore. The graph of the emission spectra is very distinctive for the type of molecule. This means that spectral imaging can be used to detect specific molecules.

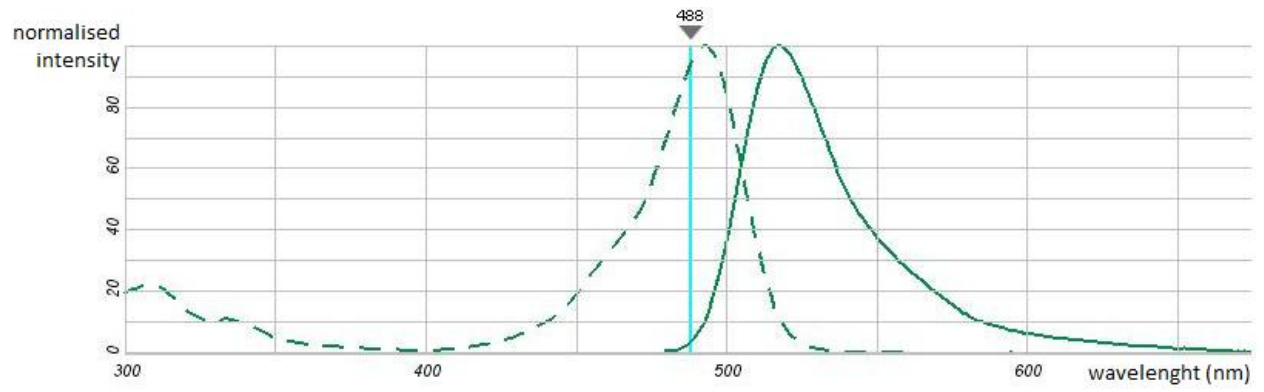


Figure 3: emission and excitation spectra of Alexa Fluor 488 hydrazide (taken from SpectraViewer, Invitrogen)<sup>11</sup>.

### 3. Experiment

The experiment is realizing a device that can excite the NADH in *in vivo* tissue with two-photons via a microendoscopic scanner. The fluorescence signal is collected and then detected, so an image of the tissue at several depths can be displayed.

The boundary conditions for this experiment are the size and mobility of the set-up, which should be able to move in the clinics. Also the set-up must be safe to use and the power of the excitation signal must be safe to use on *in vivo* tissue.

To be able to image *in vivo* tissue, we need a femtosecond pulsed laser and these pulses have to be transported towards the tissue, which process is described in more detail in Chapter 4. The pulses will enter the tissue via a scanner, developed by Philips. There are several ways to scan the tissue<sup>12</sup>, but our scanner will spirally scan the tissue and also receive the emission signal. This signal will be detected by a PMT and a CCD camera, and finally get an image by help of software. From this image we can see the morphology of the tissue and the sort of fluorophores. To get these images as clear as possible, we need to optimize the whole set-up and make sure everything is aligned properly.

We started with an existing set-up at a regular benchtop table, where we checked whether it would be possible to image with low power. If not, it would be easier to make some adjustments to the set-up on this table than on the smaller mobile table.

The samples we will use for imaging are fluorescent plastic, paper and bambooleafs. Fluorescent plastic is very easy to image and to receive signal from. Consequently this plastic is ideal for alignment of the detection. Paper has a typical structure of fibers, which can easily be imaged as well. For imaging cell morphology, we will use the leaf of a bamboo, which can easily be gathered from the university gardens. While imaging the previous samples, we will use the confocal properties of multiphoton imaging and make a z-stack, which are images of the same point in different depths.

## 4. Mobile Set-up

In this chapter the different parts of the set-up will be discussed in detail. An overview of the set-up can be seen in Fig. 4, where the different optical components are schematically displayed.

In the appendix one can read about the alignment methods for central aligning of the beam and optimizing pinholes and the fiber coupling.

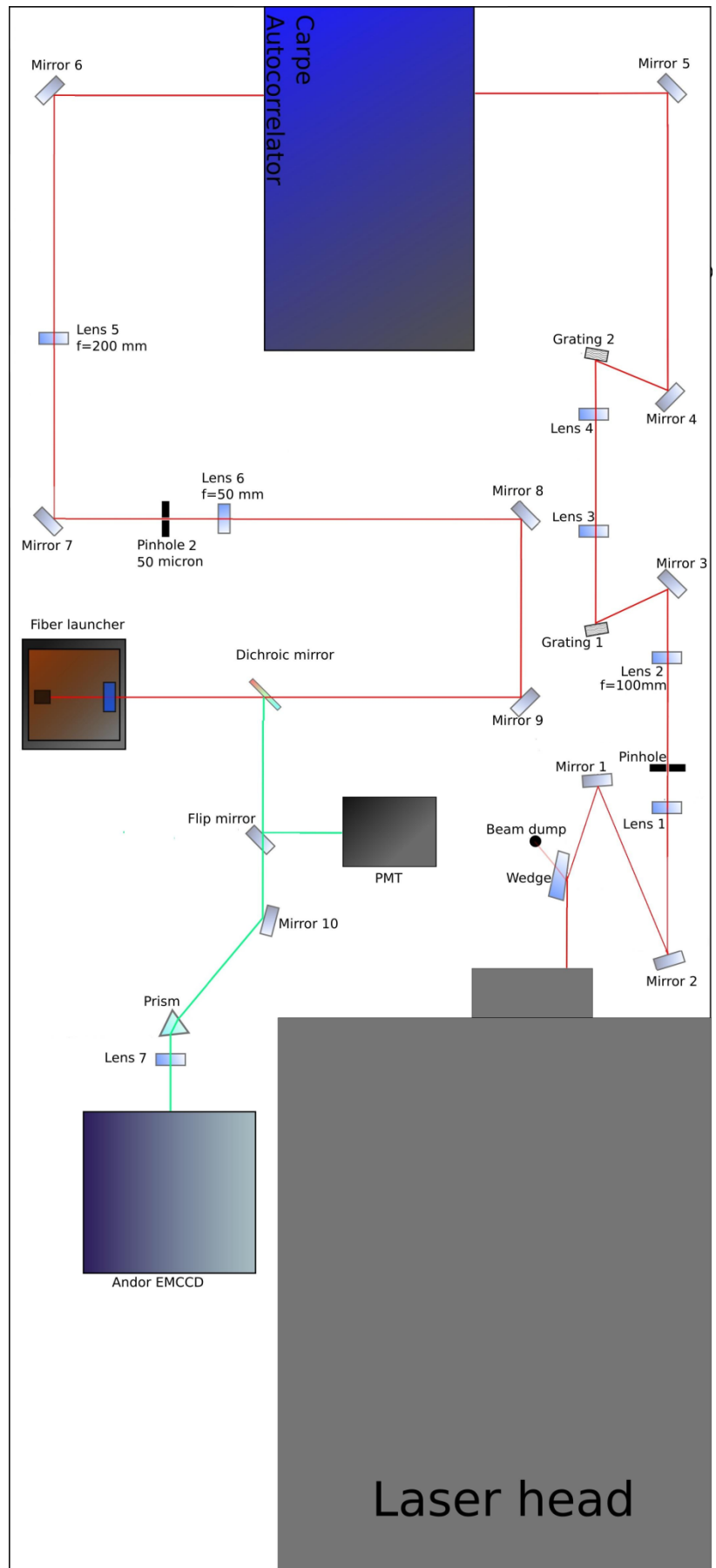


Figure 4: a schematic overview of the mobile set-up. Components and distances are not actually on scale.

## 4.1 Laser

For two-photon fluorescence one needs a pulsed laser, because of the peak in photon density. A high density of photons is needed, since two-photon excitation is a chance process and happens more often with higher photon density. A laser with femtosecond pulse widths and a high intensity is used, for a higher number of absorbed photons, so a higher emission signal. This laser we have and it is the Coherent Chameleon Titanium Sapphire (Ti:Sa) laser. The wavelength of the pulse will be around 765 nm, but it is tuneable from 680 nm up to 1080 nm. To mode-lock the beam, this laser has mirrors placed at each end of the cavity, to optimize the gain length of the amplifying medium. Since the electric field must be zero at the mirrors, boundary conditions are made and longitudinal modes are created in the cavity, such as displayed in Fig. 5. The laser has a pulse-frequency of 80 MHz.

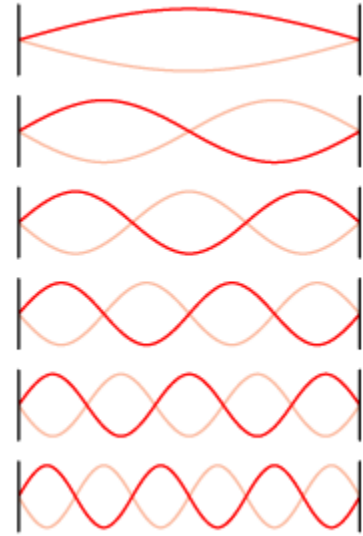


Figure 5: Different longitudinal modes in a laser cavity (taken from Wikipedia)<sup>13</sup>.

## 4.2 Attenuator

Right after the laser head, the power of the laser pulse at 765 nm is 3.4 W. This power is too high for our gratings (in the GVDC), because their gold upper layer might be damaged, so a wedge is placed to lose about 75% of the pulse its power. The amount of power loss is depending on the angle between the beam and the wedge surface. While changing the angle of the wedge minimally, the power of the beam is measured, until 76% of its initial power is lost. Now a power of 0.90 W is enough to not damage our gratings and is still high enough to detect the fluorescence signal.

## 4.3 Beam Expander

Even though the beam has just lost a lot of power, the intensity might still be too high for the gratings, because of the small surface of the beam (diameter about 2 mm). To decrease the intensity without losing its power, we will expand the beam size with two lenses with focal lengths at 30 mm and 100 mm in a Keplerian beam expander, as can be seen in Fig. 6.

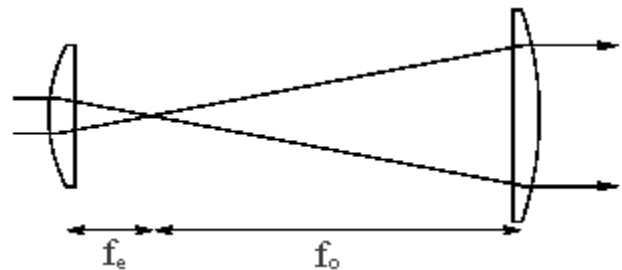


Figure 6: Keplerian beam expander with 2 convex lenses with focal points at  $f_e$  and  $f_o$  (taken from Electron6)<sup>14</sup>.

We have also placed a pinhole of 50  $\mu\text{m}$  in their mutual focal point, to get a better spot and get rid of inconvenient reflections.

## 4.4 GVDC

In the group velocity dispersion compensator (GVDC) the group velocity dispersion of the fiber will be compensated by a grating pair. This group velocity dispersion will arise in the double-clad fiber (DCF), because of the different wavelengths in our pulse will have different velocities in the fiber. The pulses will broaden due to group velocity dispersion and the eventually emitted signal will decrease because of

this pulse width. When one is using a fiber of one meter long and the inner core is pure silica, the 800 nm pulse for example will theoretically broaden from 140 fs to  $7.3 \cdot 10^2$  fs, as shown by van Weelden<sup>15</sup>.

The GVDC will split up the different wavelengths and the larger wavelengths (the red ones) will travel over a slightly larger distance, so eventually the different wavelengths will simultaneously enter the target tissue. To reduce the physical size of the already existing GVDC set-up, lenses with smaller focal lengths between the gratings are used, namely focal lengths of 50 mm instead of 100 mm.

To check whether the GVDC changes the pulse width sufficiently when the distance between the two gratings is changed, we have placed the Carpe Autocorrelator right after the GVDC. The Carpe Autocorrelator is a device which measures the pulse width of the incoming beam. We have measured the pulse widths at a wavelength of 765 nm and the results are plotted in Fig. 7. As one would expect from theory<sup>15</sup>, it is almost linear, except around the minimum, where it is merely parabolic.

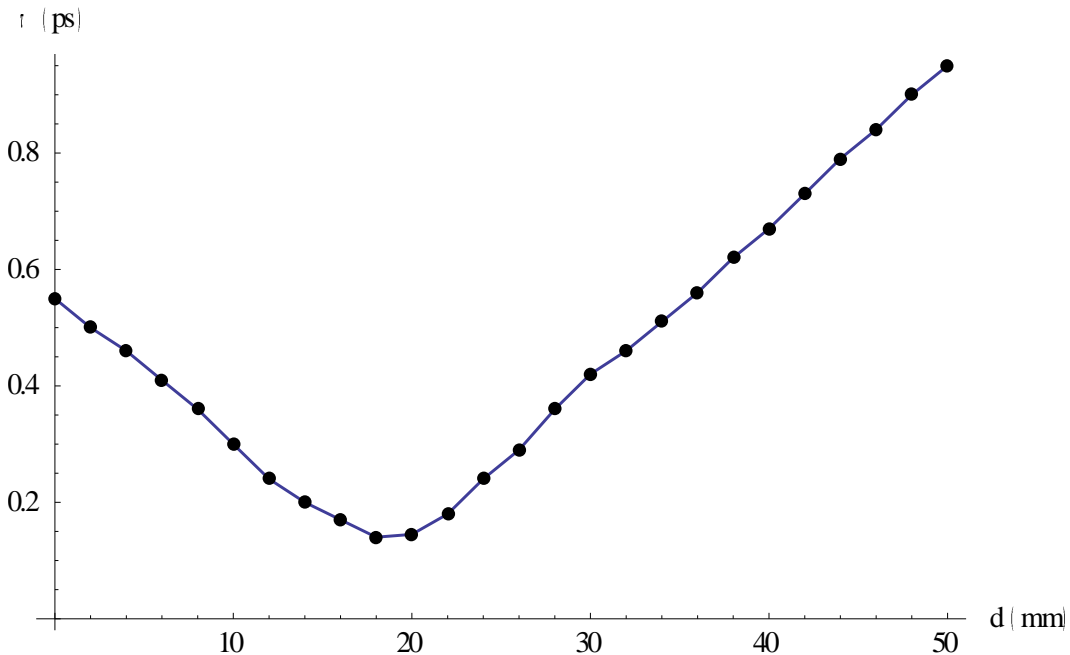


Figure 7: the pulse width (in ps) as a function of the displacement (in mm) of the gratings for 765 nm. As one could see, the GVDC is changing the pulse width. At  $d = 0$  mm the grating pair was 50 mm apart from each other.

To know at what displacement the gratings should be placed to compensate the group velocity dispersion, we used van Weelden’s experimental data<sup>15</sup>. The necessary displacement is compared with the GVDC’s minimal pulse width (for 765 nm that would be at 18 mm). The experimental data show that the grating displacement should be 27 mm for wavelengths of 730 nm and 17 mm for wavelengths of 800 nm. These displacements can be realized with our current set-up.

## 4.5 Beam Compressor and Spatial-Mode Filter

The beam compressor (BC) will compress the beam with two lenses with focal lengths at 200 mm and 50 mm. We need to compress the beam again to match the numerical aperture (NA) of the fiber core, which is 0.06. It is important to have the right beam size and NA, because otherwise one could lose a lot of laser power at the fiber coupling. One can check the NA by the following formula:

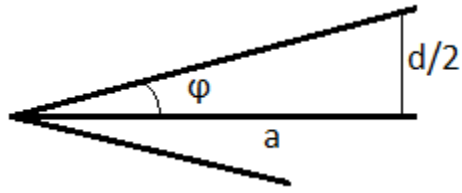


Figure 8: the specifications of angles and distances for calculating the NA.

$$NA = \sin(\varphi) = \sin\left(\tan^{-1}\left(\frac{d}{2a}\right)\right)$$

where  $a$ ,  $d$  and  $\varphi$  are the distance, diameter and angle of spot, respectively, as shown in Fig. 8. Since it is difficult to measure  $d$  and  $a$  precise, we have drawn the size the beam should have with  $NA=0.06$  and at distance  $a=140\text{mm}$ . This drawing we could keep very precise at 140mm and now we only had to look whether the actual beam matches our drawing. We could very accurately determine that this was the case and that means our NA and beam size are correct.

At exactly both the focal points of the lenses a pinhole will be placed with a diameter of  $50\ \mu\text{m}$ . This pinhole will filter out the different spatial modes of the beam, so only a single mode signal will continue. This single mode signal is needed, because of the fiber we use. To check whether the laser beam is single-mode, one could have a look at the diffraction pattern after the pinhole. If it is a single-mode signal it should have perfectly round circles and constant widths of the lines, as can be seen in Fig. 9.

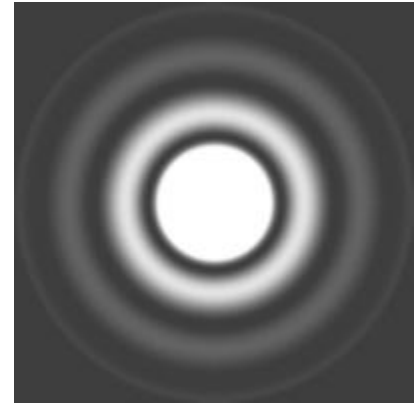


Figure 9: an example of a single-mode diffraction pattern. This pattern is also known as an Airy Pattern (taken from LaserPhysics)<sup>16</sup>.

## 4.6 Dichroic Mirror

A dichroic mirror will reflect all wavelengths under a certain value and let the higher wavelengths pass through (long pass) or the other way around (short pass). The dichroic mirror should be placed at an angle of exactly  $45^\circ$  with the beam. In our experiment we use a long pass filter, so the exciting pulse will continue through the dichroic mirror and enter the fiber via a microscope objective. The reflections of the laser pulse on the objective will also just go through the dichroic mirror, but in opposite direction, and they will hardly be reflected towards the detectors. The actual emitted light will reflect on the mirror towards the detectors, so the laser pulse is almost filtered out of the measurements.

Since the dichroic mirror does not pass 100% of the excited pulse, a small percentage will still be reflected towards the detectors. After this dichroic mirror two filters have been placed to filter out these other wavelengths travelling towards the detectors. This is to have a better noise/signal-ratio, so the images will be clearer.

## 4.7 Fiber

The fiber connects the mobile table with the handheld probe and is a double-clad photonic crystal fiber (DCF). The DCF is as well a single-mode fiber as a multimode fiber. The inner core guides the exciting, single spatial mode pulse to the probe and the inner two cores guide the returning, multimode signals. The DCF has an inner core, an inner cladding and an outer cladding with diameters of 16  $\mu\text{m}$ , 163  $\mu\text{m}$  and 315  $\mu\text{m}$ , respectively, as is displayed in Fig. 10.

The fiber will have a length of 1 m and it is very important not to bend the fiber too much, because it could break then. One may know the fiber is broken by its low power efficiency ( $\sim 0\%$ - $20\%$ ); therefore it is always important to check this efficiency regularly.

If the efficiency is low it does not immediately mean the fiber is broken. It could also be possible that the surface of the fiber is polluted and damaged by connecting the fiber to its coupling. In that case one should polish the fiber, so these scratches will disappear. It could also mean that the NA of the incoming beam does not match the NA of the fiber.

The fiber is coupled by an objective lens (Nikon S Fluor; 20x, NA 0.75). To match the NA of the fiber, the effective NA of the objective is also 0.06, by reducing the beam size. This coupling is very sensitive and

one needs a delicate stage to find the absolute power maximum of the coupling. There are different shapes possible, when measuring the power while changing  $x$ ,  $y$  or  $z$ , as can be seen in Fig. 11. When knowing the shape of the graph, one could determine whether the local maximum found is really the one you need, since there are maxima at the edges as well. Therefore it is important to always check the shape of the graph.

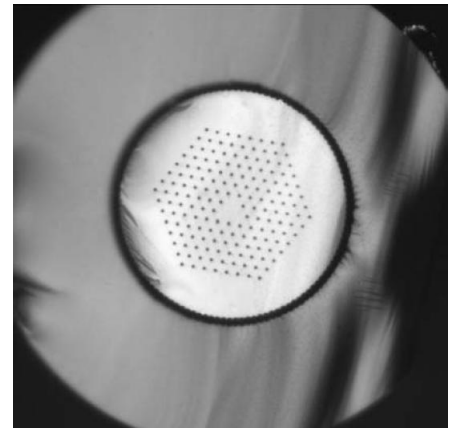


Figure 10: photograph of a photonic crystal fiber, where the core, inner and outer cladding are displayed (taken from Crystal-Fibre)<sup>17</sup>.

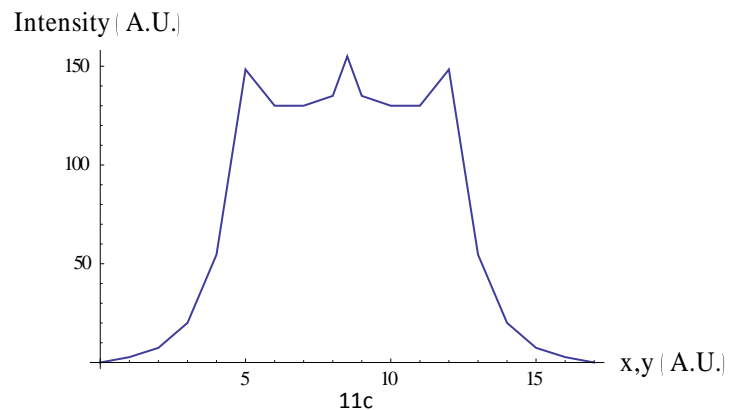
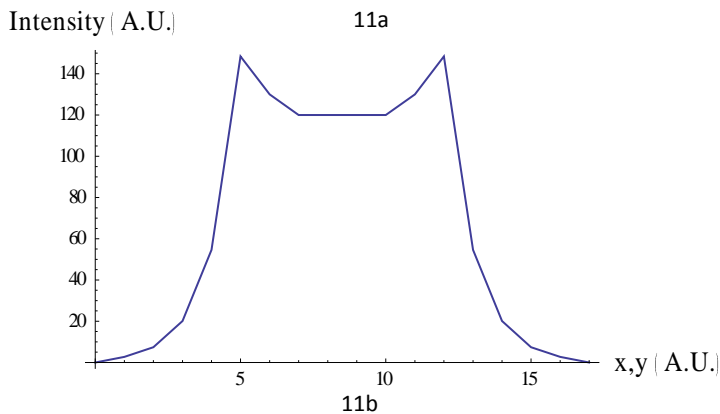
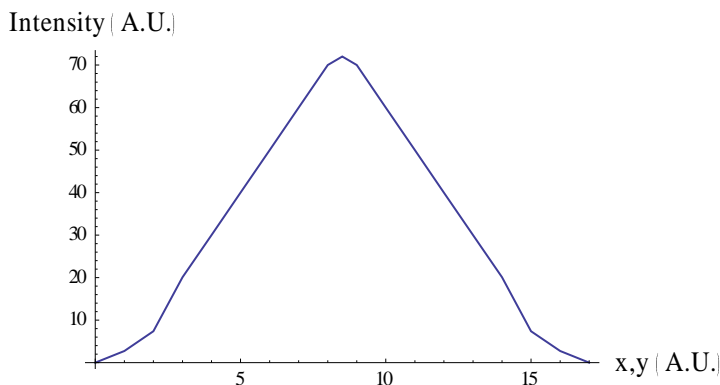


Figure 11: three possible shapes of the power intensity as a function of  $x$ ,  $y$  during the fiber coupling, with intensity profiles when not having a single-mode signal (a), having a single-mode signal but not at the right  $z$  (b) and the profile when the fiber is coupled at the right  $z$  (c). The absolute values are arbitrary, but the shape is correct.

## 4.8 Scanner

The scanner is a waterproof, compact and handheld probe designed and build by Philips, as can be seen in Fig. 12. An objective within the probe, with a free working distance in water at  $150\ \mu\text{m}$  and a NA of 0.6, is used for imaging. Inside the probe, the coils drive the magnets such that the fiber is spirally scanning the sample. This happens at a frequency of 50 Hz and we get images at a rate of one frame per two seconds, as can be read in Hendriks e.a. (2011)<sup>18</sup>. This probe emits and receives the signal while scanning and the position feedback is obtained through the coils. The head of the endoscope is small enough to use as injection, with a total diameter of 3 mm.

One cannot use too high voltages on the coils, since the fiber will hit its surroundings and it will become very hot. Once the probe is too hot, it cannot be used for *in vivo* imaging anymore, since the tissue might burn. A safety check is built in the control box so that the scanner will stop scanning at temperatures above 330 K.

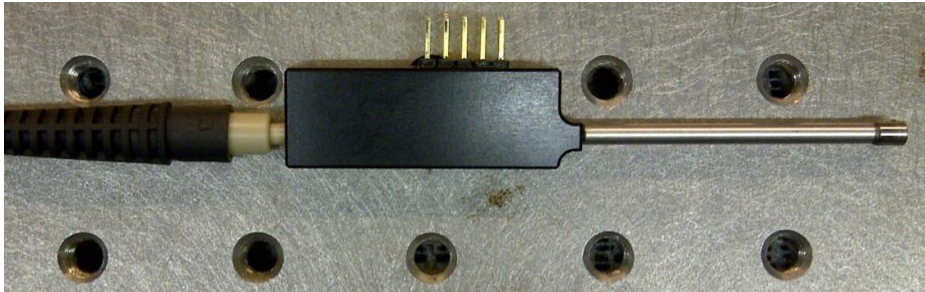


Figure 12: the scanner, placed on an optic table with 25mm distance between the holes, was made by Philips and the total diameter of the probe is 3 mm.

## 4.9 PMT detector

Once the emitted light passes the dichroic mirror there will be two possible pathways for the light to go, depending on the orientation of the flip mirror. The first path will go to a photomultiplier tube (PMT) detector. This detector can measure the intensities of the emitted light and this PMT will be used for focusing the probe correctly, because this will be a greater signal than the signal of different wavelengths. Images with this detector will display a black-and-white pattern of that layer of tissue.

To make sure the PMT will not break, but do get enough signal to image, we keep the gain at 0.50-0.70. Lower than 0.30 will probably not give any signal and higher than 1.10 will damage and eventually break the PMT.

#### 4.10 Prism and CCD camera

The other path of the flip mirror will go to a charge-coupled device (CCD) camera, via a prism to disperse the light and a lens to focus it. This is a detector for the wavelength of the emitted light, which is important to find information about the present fluorophores.

For the alignment of the CCD camera it is important to have the right angle at the prism. To calculate this angle we use Snell's Law, but we must take in account that the refractive index  $n$  is wavelength dependent. Therefore we also use the Sellmeier equation<sup>19</sup> for  $n$ :

$$n^2 - 1 = \frac{K_1 \lambda^2}{\lambda^2 - L_1} + \frac{K_2 \lambda^2}{\lambda^2 - L_2} + \frac{K_3 \lambda^2}{\lambda^2 - L_3}$$

where the constants  $K_1, K_2, K_3, L_1, L_2, L_3$  are depending on the sort of glass used. For alignment, the average wavelength should be parallel to one surface of the prism, so that  $\beta = 0$ , as shown in Fig. 13. With Sellmeiers equation and Snell's Law, one can calculate  $\beta$  at different wavelengths and for different  $\alpha$ <sup>20</sup>, as can be seen in Fig. 14. From this figure one could see that at  $\alpha = 19.5^\circ$  the angle  $\beta$  will be zero for a wavelength of 510 nm, which is average enough for our measurements.

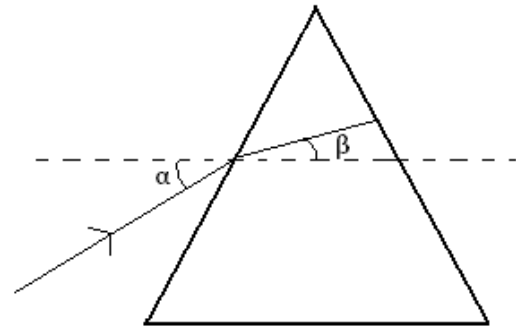


Figure 13: a prism with the angles  $\alpha$  and  $\beta$  shown.

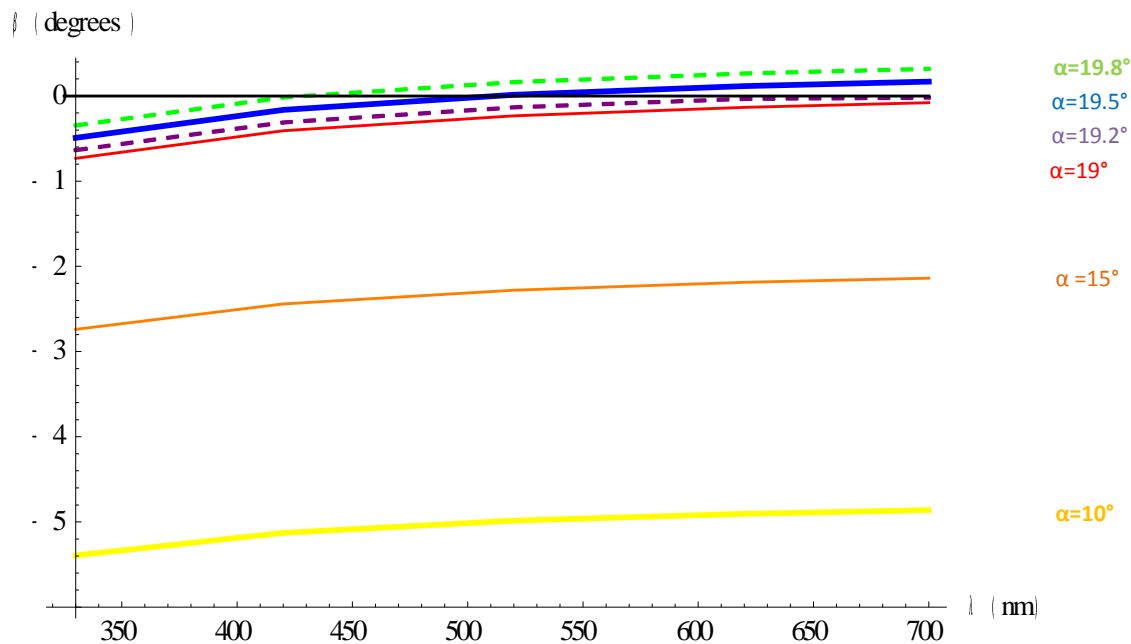


Figure 14: graphs of the angle inside the prism as a function of the wavelength. The different colors indicate different incident angles, with yellow at  $\alpha=10^\circ$ , orange at  $\alpha=15^\circ$ , red at  $\alpha=19^\circ$ , purple (dashed) at  $\alpha=19.2^\circ$ , blue at  $\alpha=19.5^\circ$  and green (dashed) at  $\alpha=19.8^\circ$ .

## 5. Results

### 5.1 Regular Benchtop Set-up

Fig. 15 is the two-photon fluorescence image of a bamboo leaf. On the left side one could see the leaf's cell structure. The thick black stripe on the right side of the image is one of the leaf's veins. In these veins water is transported, which is not an intrinsic fluophore, so it will be displayed black on a two-photon fluorescence image.

Since two-photon fluorescence provides a confocal image, we are able to image different layers of the tissue. This can be seen in Fig. 16, where the different layers of the bamboo leaf are visible. Since the leaf did not have a flat surface, one can see in Figs. 16(m)-16(r) that different parts of the same cellular layer are focused at different depths.

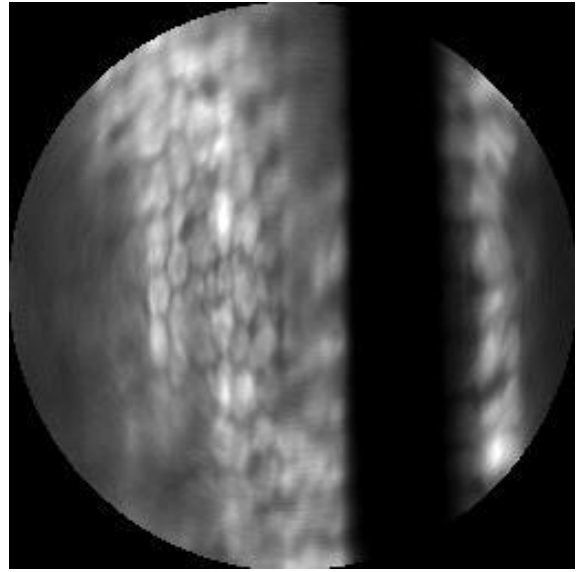


Figure 15: two-photon fluorescence image of bamboo leaf of  $175 \times 175 \mu\text{m}$ , at  $65 \mu\text{m}$  depth from the surface. For these images an excitation wavelength of  $765 \text{ nm}$  and an excitation power on the sample of  $13 \text{ mW}$  were used. Detection is done with a PMT and gain of  $0.40$  (made March 2<sup>nd</sup> 2012).

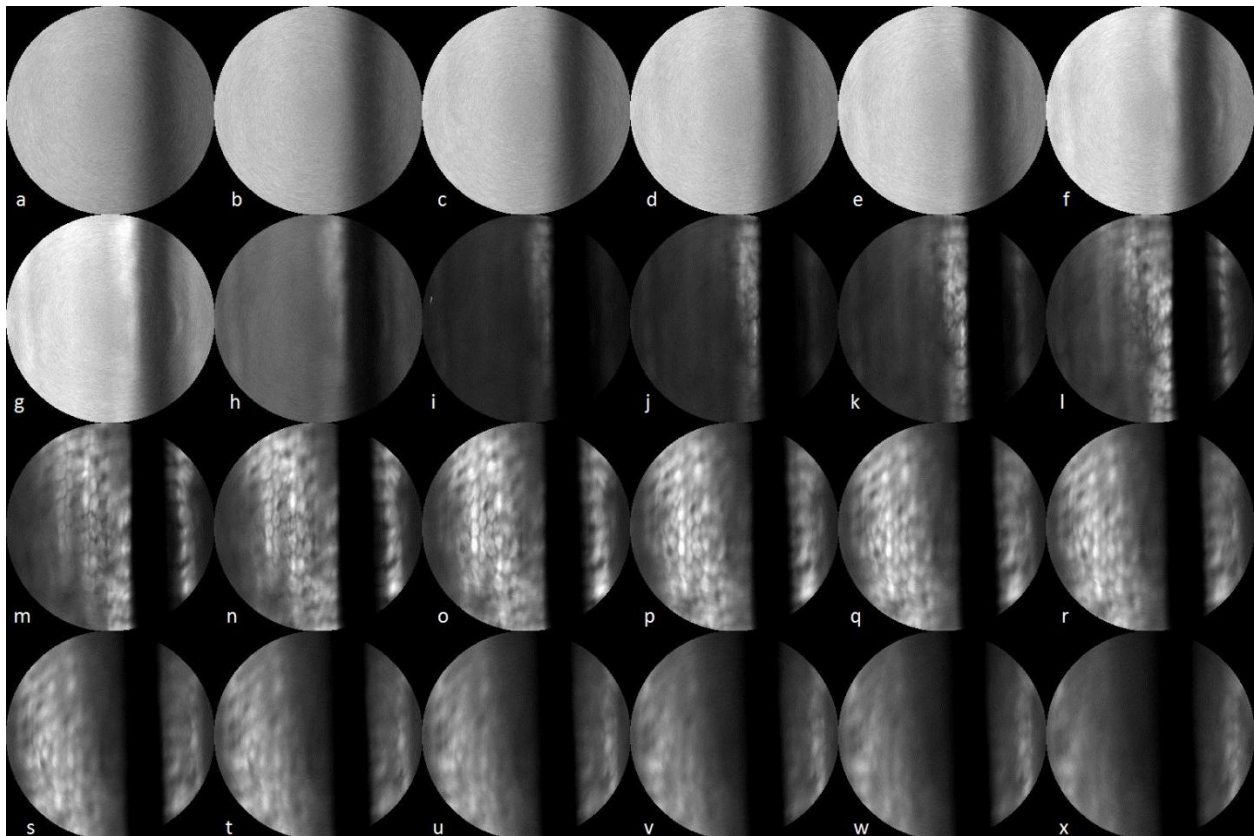


Figure 16: two-photon fluorescence images of bamboo leaf of each a  $175 \times 175 \mu\text{m}$  field of view. These images were made at different depths of the tissue, starting at  $0 \mu\text{m}$  till  $115 \mu\text{m}$  from the surface. For these images an excitation wavelength of  $765 \text{ nm}$  and an excitation power on the sample of  $13 \text{ mW}$  were used and the detection is done with a PMT with gain of  $0.40$  (made March 2<sup>nd</sup> 2012).

## 5.2 Mobile Set-up

Fig. 17 is the two-photon fluorescence image of paper. One can see the different layers of fibers of the paper. This image is made with a PMT detector, with its gain at 0.51 V.

The little black spots in the outer circles of the image are caused by the inaccurate scanning of the fiber. The scanner scans 1660 points per round, but the image is expected to be 256 pixels width, so some pixels have not been appointed any value and therefore stay black. One can set the scanner at more points per round and thereby lose the black spots in the image, but it will acquire longer to make an image.

Also for paper, we are able to image different layers of the sample. This can be seen in Fig. 18, where the different layers of the fibers of paper are visible. The difference between two sequential images is 5  $\mu\text{m}$  and the difference between Fig. 18(a) and Fig. 18(t) is 100  $\mu\text{m}$ . These images were also made with a PMT detector, with its gain at 0.51.

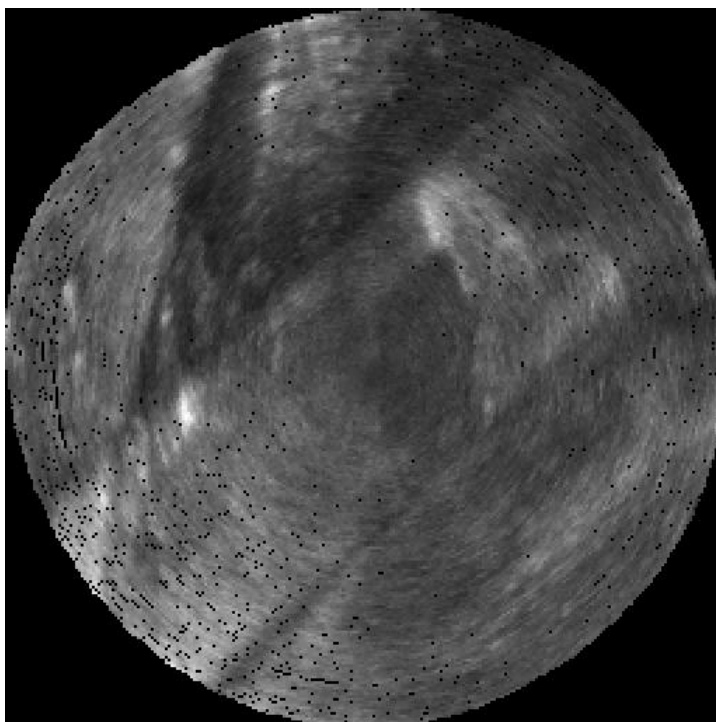


Figure 17: two-photon fluorescence image of paper with a 175x175  $\mu\text{m}$  field of view. For these images an excitation wavelength of 770 nm and an excitation power on the sample of 9.0 mW were used. Detection is done by a PMT (made July 3<sup>rd</sup> 2012).

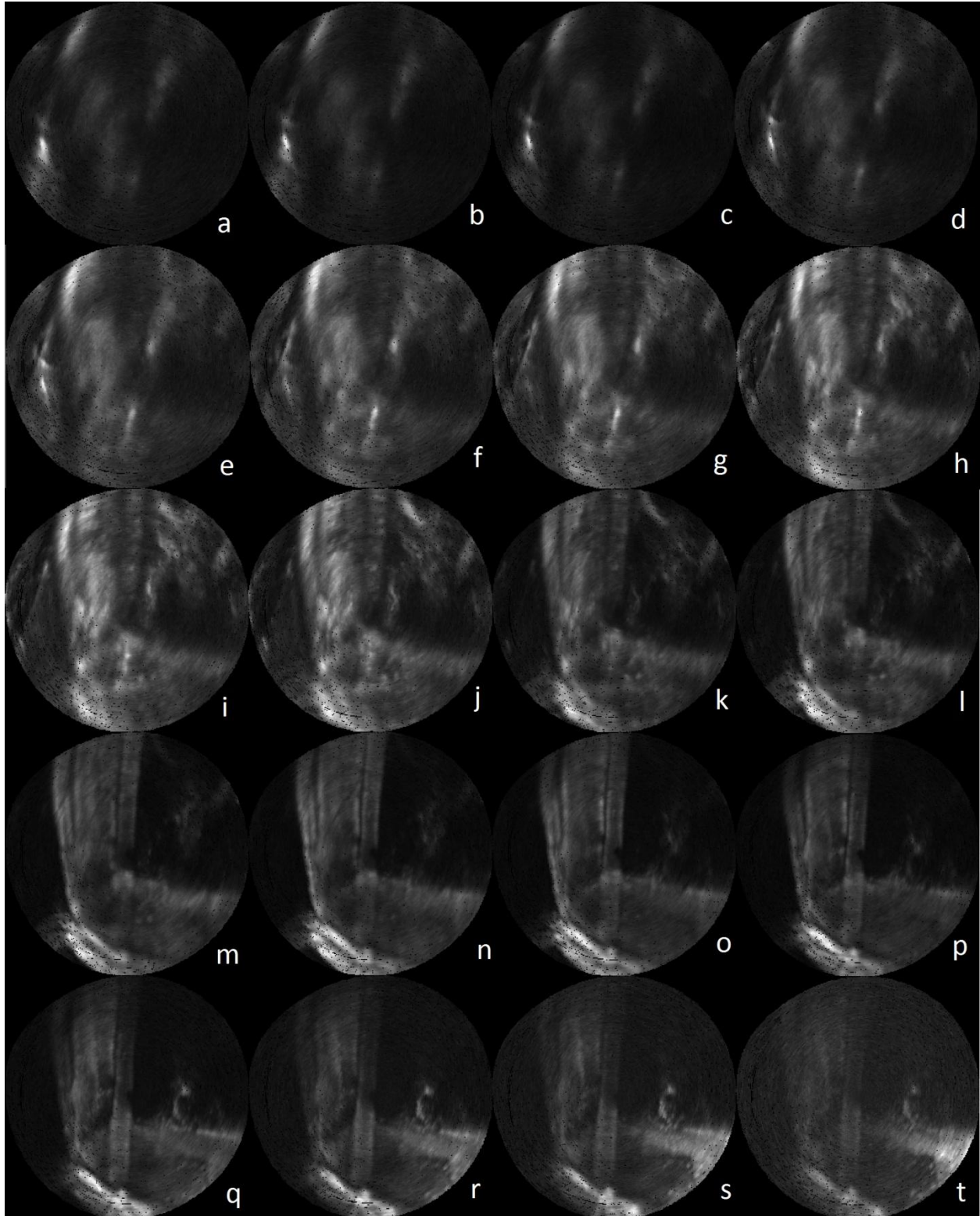


Figure 18: two-photon fluorescence image of paper with a  $175 \times 175 \mu\text{m}$  field of view. These images were made at different depths of the sample, with steps of  $5 \mu\text{m}$  per image. For these images an excitation wavelength of  $770 \text{ nm}$  and an excitation power on the sample of  $9.0 \text{ mW}$  were used. Detection is done by a PMT (made July 3<sup>rd</sup> 2012).

## 6. Further research

Although the mobile set-up produces images, it still needs optimization before it can be used in clinics. Especially a higher signal/noise-ratio will yield better images. The noise is mainly produced by the excitation laser light and probably comes from reflections on the objective and dichroic mirror. One should try to block the excitation signal and its reflections towards the detection, without losing signal.

Furthermore, we have not yet been able to align the CCD camera, which is very important for analyzing the fluorophores. The PMT detector can be used for imaging the morphology of the tissue, but to know the actual fluorophore, one needs the spectral information which can be obtained by the CCD camera.

At last, the mobile table can be prepared for going into the clinics. This means the whole set-up will be covered, so the laser light cannot cause any damage due to its high power and no dirt can enter the set-up.

## 7. Conclusion

Concluding, I can say that although my two-photon fluorescent images with the mobile table are not yet of an *in vivo* sample, this bachelor research proved to be a useful experience. I have learned a lot about doing research, which cannot be taught by normal courses, and therefore prepared myself for doing a master. Not only have I learned a lot about the subject I investigated, I also learned a lot about writing reports and presenting results, but also picked up a few things about microscopes, collagen, fungi and much more biological subjects. I hope this report reflects the things I've learned and the effort I put into it.

## 8. Acknowledgements

I would like to thank Hans Gerritsen for his help and input on the prism calculations, which allowed me to build that part of the set-up. Furthermore, I would like to thank Oleg Nadyarnykh for his help during the vacation of Johan. Last but not least I would like to thank Johan for his efforts to explain everything to me and his good taste of music in the lab.

## 9. Appendix

### 9.1 Periodic check

Aligning and optimizing the beam and the optical components should be checked before starting anything else and is described in this appendix. One can easily check the central alignment of the beam at the three cages, namely in the beam expander, GVDC and beam compressor, with a target.

Afterwards one should optimize the pinholes with the laser in alignment mode, starting with the one in the beam expander and then the one in the beam compressor. Then one should also check the central alignment of the objective, using the target and the mirror in tube. Afterwards one can start optimizing the fiber coupling.

Since the pinholes and fiber coupling are very delicate optical instruments, one should check their optimization every 30 minutes when using the set-up.

### 9.2 Constant height beam

Mirrors are used to change the direction of the beam, but do not reflect all the light. For having the reflection efficiency as high as possible, one should use the mirrors matched with the wavelength of the beam. Since all our optical components are at the same height, so in the same plane, it is important to have the mirrors reflect the beam only in that plane. To check whether a mirror is perpendicular to the optical plane, one places the mirror right in front of the beam, so that the beam will be reflected towards its original source. If the reflected beam ends up at the same height as its source, the mirror will be perpendicular to the optical plane. For more precise results, one should enlarge the distance between the mirror and the beam source.

### 9.3 Center alignment beam

For lenses and other optical components it is important that the beam goes right through the middle of the component. This means that not only the position should be right, but also the incoming angle. Therefore one uses two mirrors, as can be seen in Fig. 19. The first mirror is used for the location of the beam, while the second mirror is used for the angle. Fig. 19 shows the different effects of those two mirrors, where in Fig. 19(a) the original beam path is displayed. In Fig. 19(c) only the second mirror has changed and in Fig. 19(b) the first mirror has changed, but the second one needs to change as well to have the beam parallel to its original path.

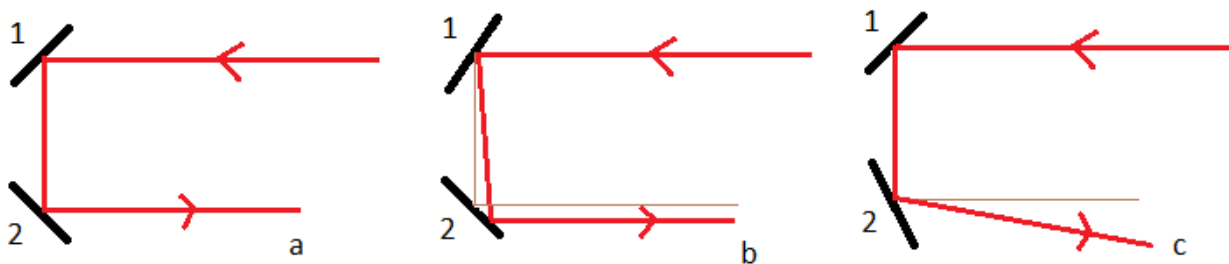


Figure 19: a schematic overview from above, of changing the direction of the beam by two mirrors. In (a) the original beam is displayed and in (b) and (c) the mirrors 1 and 2, and the mirror 2 has been changed, respectively.

One can align the beam in different ways. One could use two targets, which are alignment instruments to indicate the middle of the cage. One of those targets is placed close to the second mirror and for the alignment of this target mirror 1 is used. The other target is placed farther away of the second mirror and is used for checking the angle of the beam. This target will be aligned with mirror 2. One will have to keep switching between the targets and mirrors until finally an optimal alignment is achieved.

The other type of alignment of the beam is by use of a target and a mirror. This target can be mounted to a tube with a mirror. The target can be aligned with mirror 1 and the mirror in the tube will give a total reflection, which can be used for alignment of the angle by mirror 2.

#### **9.4 Optimizing pinhole and fiber coupling**

A pinhole can be aligned and optimized by mounting it on a holder which can be tuned very accurately in x- and y-direction. One places a power meter behind the pinhole and starts turning one of the two screw caps, until a maximum is found. Then one starts turning the other screw cap until again a maximum is found. Afterwards one will turn both of the screw caps even more, so the actual optimal is reached.

The fiber coupling can be optimized when it is mounted on a delicate stage which can be tuned very accurately (sub-micron) in x-, y- and z-direction. One places a power meter at the end of the fiber so that the power meter is placed at a maximum. Afterwards one starts tuning the different x- and y-directions, until a maximum is reached. Then one changes the coupling in the z-direction and tunes the x- and y-directions again until a maximum is reached. Once one finds the intensity profile as in Fig. 11(c), one has found the right z.

## 10. References

---

- <sup>1</sup> Bao, H., Allen, J., Pattie, R., Vance, R. and Gu, M. (2008). Fast handheld two-photon fluorescence microendoscope with a 475  $\mu\text{m}$  x 475  $\mu\text{m}$  field of view for in vivo imaging. *Optic Letters*, Vol. 33, No. 12, 1333-1335.
- <sup>2</sup> Bader, A. N., Pena, A., Voskuilen, C.J. van, Palero, J.A., Leroy, F., Colonna, A. and Gerritsen, H.C. (2011). Fast nonlinear spectral microscopy of in vivo human skin. *Biomedical Optics Express*, Vol. 2, No. 2, 365-373.
- <sup>3</sup> Rivera, D. R., Brown, C. M., Ouzounov, D. G., Pavlova, I., Kobat, D., Webb, W. W. and Xu, C. (2011). Compact and flexible raster scanning multiphoton endoscope capable of imaging unstained tissue. *PNAS*, Vol. 108, No. 43, 17598-17603.
- <sup>4</sup> Lakowicz, J. R. (2006). *Principles of Fluorescence Spectroscopy*. Springer Science+Business Media, LLC, New York.
- <sup>5</sup> So, P.T.C., Dong, C.Y., Masters, B.R., Berland, K.M. (2000). Two-photon excitation fluorescence microscopy. *Annual Reviews: Biomedical Eng*, No. 2, 399-429.
- <sup>6</sup> Denk, W., Strickler, J.H., Webb, W.W. (1990). Two-photon laser scanning fluorescence microscopy. *Science*, Vol. 248, 73-76.
- <sup>7</sup> Wikipedia: [http://en.wikipedia.org/wiki/File:Second\\_Harmonic\\_Generation.svg](http://en.wikipedia.org/wiki/File:Second_Harmonic_Generation.svg), visited June the 12<sup>th</sup> 2012.
- <sup>8</sup> Berg, J.M., Tymoczko, J.L., Stryer, L. (2007). *Biochemistry*. W.H. Freeman and Company, New York, 6<sup>th</sup> edition. Chapter 15 (p420-421), 16 (p436-446), 17 (p489) and 18 (p503, 507-509).
- <sup>9</sup> Warburg, O. (1956). On the origin of cancer cells. *Science*, Vol. 123 (3191), 309-314.
- <sup>10</sup> Jones, P.A., DeClerck, Y.A. (1980). Destruction of extracellular matrices containing glycoproteins, elastin and collagen by metastatic human tumor cells. *Cancer Research*, No. 40, 3222-3227.
- <sup>11</sup> Invitrogen: <http://www.invitrogen.com/site/us/en/home/support/Research-Tools/Fluorescence-SpectraViewer.html>, visited July the 3<sup>rd</sup> 2012.
- <sup>12</sup> Flusberg, B.A., Cocker, E.D., Piyawattanametha, W., Jung, J.C., Cheung, E.L.M. and Schnitzer, M.J. (2005). Fiber-optic fluorescence imaging. *Nature Methods*, Vol. 2, No. 12, 941-950.
- <sup>13</sup> Wikipedia: <http://en.wikipedia.org/wiki/File:Longitudinal-mode.png>, visited June the 8<sup>th</sup> 2012.
- <sup>14</sup> Electron6: <http://electron6.phys.utk.edu/optics421/Laboratories/Lab2.htm>, visited June the 8<sup>th</sup> 2012.
- <sup>15</sup> Weelden, J. van (2010). *Instrumentation of a group velocity dispersion compensator*. Master thesis, Utrecht University.

- 
- <sup>16</sup> LaserPhysics: <http://laser.physics.sunysb.edu/~marissa/report/>, visited June the 28<sup>th</sup> 2012.
- <sup>17</sup> Crystal-Fibre: photograph from data sheet, supplied by manufacturer. October 16<sup>th</sup> 2009.
- <sup>18</sup> Hendriks, B.H.W., Bierhoff, W.C.J., Horikx, J.J.L., Dejardins, A.E., Hezemans, C.A., 't Hooft, G.W., Lucassen, G.W., Mihajlovic, N. (2011). High-resolution resonant and nonresonant fiber-scanning confocal microscope. *Journal of Biomedical Optics*, vol. 16(2), 026007-1–026007-8.
- <sup>19</sup> Hecht, E. (1998). *Optics*, third edition, chapter 3. Addison Wesley Longman, Inc., Reading Massachusetts.
- <sup>20</sup> Via internal communication with Hans Gerritsen.